Microexplosion of aluminum slurry droplets

Do Young Byun, Seung Wook Baek*, Ju Hyeong Cho

Aerospace Engineering Department, Korea Advanced Institute of Science and Technology, 373-1 Kusong-Dong, Yusung-Gu, Taejon, 305-701, South Korea

Abstract

The microexplosion of a slurry droplet is experimentally and theoretically investigated. The microexplosion was considered to be caused by the shell formation and the following pressure build-up in the shell which would be promoted by the suppression of evaporation, subsequent superheating and heterogeneous nucleation of a liquid carrier. Experimentally, the microexplosion phenomena was examined for various surfactant concentrations and particle loading under different ambient temperature ranges (500–900 K). To closely investigate the pressure build-up and the heterogeneous nucleation, a numerical model was introduced by considering the three stages such as the shell formation, suppression of evaporation and pressure build-up inside. The microexplosion time was estimated by postulating the limit of superheat for heterogeneous nucleation. The simulation yielded a reasonably good agreement with experimental results for Al/*n*-heptane slurry droplets under various solid loadings (10–40 wt.%). © 1999 Elsevier Science Ltd. All rights reserved.

1. Introduction

Slurry fuels have drawn substantial attention during several decades on account of their potential advantage as high-energy-density fuels for volume-restricted air-breathing propulsion systems. These potentials, however, may be somewhat difficult to accomplish because the burning of the agglomerates created by consuming liquid fuel carrier is rather slow compared with the liquid fuel burnout period [1]. Recently, many researches on the burning of various slurry fuels have shown that the microexplosion of slurry droplets with some pertinent additives is a possible remedy for the difficulties mentioned above, for the microexplosion is followed by shattering of parent droplets into many small ones, thereby making much larger surface areas

of slurry droplets available. Moreover, the microexplosion of slurry droplets can reduce the corrosion of the inner wall of combuster as well as the generation of some pollutants which may be caused by inefficient combustion.

As already observed for the slurry droplets [2–8], a shell is formed at the droplet surface with the help of high-boiling point and low volatile surfactants, as the liquid carrier in slurry droplet evaporates. This shell delays the evaporation of the liquid carrier so that the pressure inside the droplet builds up until the shell is shattered.

Takahashi et al. [3,4] proposed a microexplosion mechanism based on the experimental combustion of Boron/JP-10 slurry droplets. The pressure inside the droplet was found to build up enough to promote the microexplosion when the surface temperature of the slurry droplet reaches the point at which the weight loss by pyrolysis of surfactant amounts to 5–10%. The procedure was discussed by defining the d^2-law combustion stage, shell formation stage, and disruption

---

* Corresponding author. Tel.: +82-42-869-3714; fax: +82-42-869-3710.

E-mail address: swbaek@sorak.kaist.ac.kr (S.W. Baek)

Nomenclature

A_d	pre-exponential factor	λ	thermal conductivity
C	specific heat	μ	viscosity of fuel gas
D	diffusion coefficient	μ_{sto}	stoichiometric coefficient of oxygen
e	emissivity of the droplet surface and heater	ρ	density
E	activation energy	σ	Stefan–Boltzmann constant, 5.6696×10^{-8}
l_{sh}	accumulated shell thickness		$W/m^2\,K^4$
L	latent heat of vaporization of fuel	ϕ	solid volume fraction
MW	molecular weight	ω	solid mass fraction.
p	pressure		
q	heat flux	*Subscripts*	
Q	heat of reaction of liquid fuel	co	nonaccumulated core of the droplet
r	r-coordinate from the droplet center	F	fuel
R_U	universal gas constant, 8314 J/kmol K	g	gas
t	time	li	liquid
T	temperature	N_2	nitrogen
T_B	boiling point of liquid fuel	O	oxygen
T_h	temperature of heater wall	s	solid or droplet surface
V	gas velocity	sg	binary mixture of solid and gas
Y	mass fraction.	sh	accumulated shell
		sl	binary mixture of solid and liquid
Greek symbols		0	initial condition
ε	porosity	∞	infinite condition.

stage. Lee and Law [9] showed that these three stages could also apply to the results with Carbon/JP-10 slurry droplets. Cho et al. [7], based on the concept suggested by Takahashi et al. [4], calculated the disruption time of a slurry droplet with the assumption that the critical surface temperature for the disruption is equal to the pyrolysis temperature of the surfactant at which 5 to 10% weight loss of the surfactant is attained in the curve of the TGA (thermogravimetric analysis) [4]. Based on the experiments with Al/JP-10 slurry droplets, Wong and Lin [5] observed that the droplet surface temperature could exceed the boiling point of JP-10, and the droplet was shattered when the temperature at $r = 0.8r_s$ reached the boiling point of JP-10. Therefore, the attainment of superheating and heterogeneous nucleation of the liquid carrier was found to be as important as the impermeable shell formation.

Even if the previous studies [4,5,7] introduced the importance of the heterogeneous nucleation, no prediction of the microexplosion time was discussed using this phenomenon as criteria and prediction of the disruption time was just investigated. In this paper, it is intended to quantitatively investigate each of the heating, shell formation, pressure build-up, and heterogeneous nucleation processes involved in the microexplosion phenomena, based on the extended modeling as well as the experiments. The microex-

plosion time was estimated by postulating the limit of superheat for heterogeneous nucleation. The predicted results are then compared with the experimental ones.

2. Experimental methods

2.1. Test apparatus

The microexplosion of a slurry droplet is investigated by heating the droplet formed around a tiny ceramic ball attached to a quartz fiber with diameter of 100 μm. Thereby, a nearly spherically shaped droplet could be obtained.
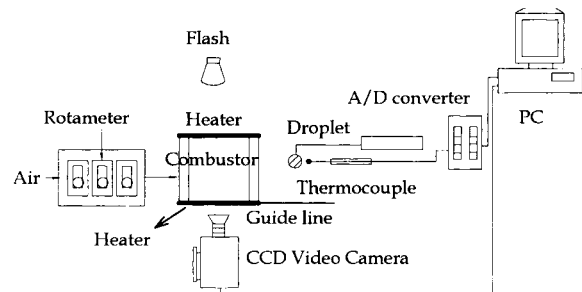
Fig. 1 shows a schematic of the experimental appar-
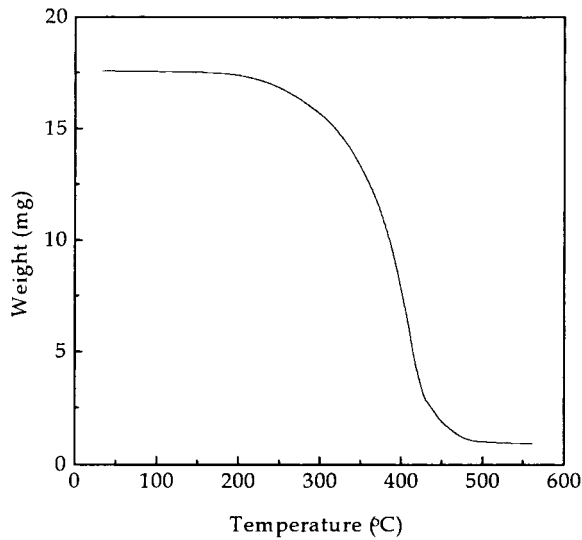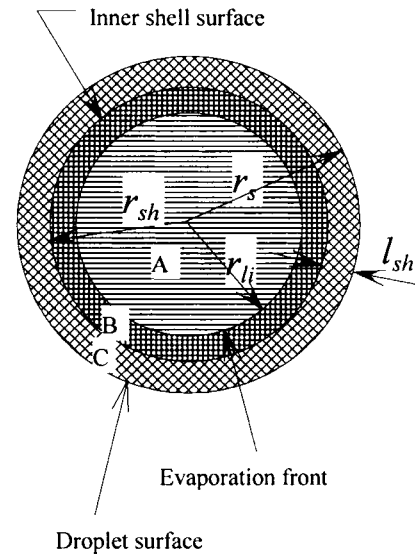

Fig. 1. Schematic diagram of the experimental setup.

Fig. 2. Thermogravimetric analysis of surfactant (SPAN 85).

Fig. 3. Schematic of a slurry droplet.

atus used here. The combustor consists of quartz windows and two electric radiators placed at both top and bottom sides of the combustor. A suspended droplet is introduced into the hot environment inside the combustor by quickly moving the whole combustor setup along the guided track. The microexplosion and the combustion processes are recorded by CCD camera (Sony CCD-V5000) with the backlight in order to get the shadow effect. The explosion time as well as the droplet diameter variation is determined by examining a temporal change of droplet images. The effective droplet diameter is determined by approximating its image as ellipsoid. When a droplet is exposed to the hot environment, it is heated both convectively and radiatively by the electric radiators. This requires an experimental determination of the surface wall temperature of the heater as well as the gas temperature. Temperatures are measured using an SiO_2 coated Pt/ Pt-13%Rh thermocouple (25 μm) by considering radiative heat loss correction. The emissivity of the heater is measured using the one-color pyrometer.

2.2. Slurry samples

Slurry samples are prepared by mixing aluminum powders with *n*-heptane and a small amount of surfactant (Sorbitan Trioleate, SPAN 85) added. The boiling temperature of *n*-heptane is 371 K. The Al particles with mean diameter of about 5 μm are dried in an oven at 150°C for several hours. While the solid loading varies from 10 to 40 wt.%, the surfactant loading ranged from 0.5 to 4 wt.%. The thermal decomposition of the surfactant is characterized using TGA (thermogravimetric analysis), as shown in Fig. 2. In
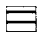
this study, the temperature of 492 K corresponding to a 2% weight loss of surfactant is selected as the reference temperature for surfactant pyrolysis following the definition by Wong et al. [6].

3. Theoretical formulation

3.1. Assumptions and governing equations

The following assumptions are made to simulate the evaporation and the microexplosion processes of the slurry droplet.

1. The droplet is spherically symmetric and convection is neglected.
2. Initially, the solid particles are uniformly distributed inside the droplet and their total weight is preserved constant during evaporation.
3. The accumulated shell thickness increases with a fixed porosity during evaporation.

A schematic of the evaporating slurry droplet in Fig. 3 comprises three regions, A, B, and C. While the region

A indicates the slurry region (solid + liquid), B and C indicate the porous region (solid + gas). The porosity of A and B is identical with the initial value of the slurry droplet ($\varepsilon = \varepsilon_{co}$). The accumulated shell region, C, has the porosity of ε_{sh} which is smaller than ε_{co}. The accumulated shell thickness, l_{sh}, is then calculated by

$$l_{sh} = r_s - \left(\frac{(1 - \varepsilon_{sh})r_s^3 - (1 - \varepsilon_{co})r_0^3}{\varepsilon_{co} - \varepsilon_{sh}} \right)^{1/3} \tag{1}$$

where r_0 and r_s represent the initial droplet radius and the transient droplet radius during shell formation stage, respectively. The governing equations are as follows.

For the slurry region (solid + liquid): $0 < r < r_{li}$.

For the region inside the liquid evaporation front, the following energy conservation equation applies

$$(\rho C)_{sl} \frac{\partial T}{\partial t} = \frac{\lambda_{sl}}{r^2} \frac{\partial}{\partial r} \left(r^2 \frac{\partial T}{\partial r} \right) \tag{2}$$

where the subscript 'sl' represents a binary mixture of solid particles and liquid carrier. Their mixture properties are calculated by the procedure of Lee and Taylor [10].

For the porous region as well as the gas field outside the droplet: $r_{li} < r$.

Right from the evaporation front to the outward direction, the gaseous species exist all the way from the porous region to the gas phase region outside the droplet boundary. In this zone, the following mass, energy, and species equations are considered for both the porous region ($\varepsilon = \varepsilon_{sh}$) and the gas field ($\varepsilon = 1$) [11]:

Continuity:

$$\varepsilon \frac{\partial \rho_g}{\partial t} + \frac{1}{r^2} \frac{\partial}{\partial r}(\varepsilon r^2 \rho_g V) = 0 \tag{3}$$

Energy:

$$(\rho c)_{sg} \frac{\partial T}{\partial t} + \varepsilon(\rho c)_g V \frac{\partial T}{\partial r}$$
$$= \frac{1}{r^2} \frac{\partial}{\partial r} \left(r^2 \lambda_{sg} \frac{\partial T}{\partial r} \right) + \varepsilon(MW)_F Q \dot{w} \tag{4}$$

Species:

$$\rho_g \frac{\partial Y_i}{\partial t} + \rho_g V \frac{\partial Y_i}{\partial r}$$
$$= \frac{1}{\varepsilon} \frac{1}{r^2} \frac{\partial}{\partial r} \left(\varepsilon r^2 \rho_g D_i \frac{\partial Y_i}{\partial r} \right) - (MW)_i \dot{w}, \tag{5}$$
$$i = \text{fuel}$$

$$\rho_g \frac{\partial Y_i}{\partial t} + \rho_g V \frac{\partial Y_i}{\partial r}$$
$$= \frac{1}{\varepsilon} \frac{1}{r^2} \frac{\partial}{\partial r} \left(\varepsilon r^2 \rho_g D_i \frac{\partial Y_i}{\partial r} \right) - \mu_{sto}(MW)_i \dot{w}, \tag{6}$$
$$i = \text{oxygen}$$

Equation of state:

$$\rho_g = \frac{p(MW)_g}{R_U T} \tag{7}$$

Table 1
Physical properties and parameters

	Parameters	Unit	Value
n-Heptane [17]	A_d	kg^2 m^3/kmol^3 s	0.8×10^6
	C_p	J/kg K	2310
	E	J/kmol	0.7×10^8
	MW	kg/mol	100
	Q	J/kg	4.46×10^7
	μ_{sto}		11
	μ	N/m^2 s	1×10^{-5}
	T_B	K	371.55
	λ [16]	W/m K	$0.265 - 6.4048 \times 10^{-4}T + 5.9524 \times 10^{-7}T^2$ (280 K $< T <$ 400 K)
	L	J/kg	$55536.37(540 - T)^{0.3436}$
	ρ [18]	kg/m^3	$965.276 - 0.9543\,T$ (273.15 K $< T <$ 443.15 K)
Al [18]	C_p	J/kg K	997
		W/m K	236
	ρ	kg/m^3	2702

Pressure build-up [12]:

$$\varepsilon V = -\frac{K}{\mu}\nabla p \tag{8}$$

where

$$K = \frac{d_s^2 \varepsilon^3}{180(1-\varepsilon)^2} \tag{9}$$

The subscript 'sg' represents a solid and gas mixture and their properties are calculated by the procedure of Cho et al. [7] and Kunii and Smith [13]. Mass diffusion coefficients for fuel, D_F, and oxygen, D_O, in Eqns. (5) and (6) can be found in Fuller et al. [14]. As shown in equations (8) and (9), from the Darcy law in the porous media, the volumetric force balance can be expressed using the bulk resistance characterized by the viscosity of the Newtonian fluid μ and the permeability of the solid matrix K [12].

The reaction rate term $\dot{w}$ in Eqns. (4)–(6) can be given by the single step second-order reaction equation [15].

$$\dot{w} = \frac{A_d \rho_g^2 Y_O Y_F}{(MW)_O (MW)_F} \exp\left(-\frac{E}{R_U T}\right) \tag{10}$$

Physical properties required for modeling are listed in Table 1.

3.2. Initial and boundary conditions

The initial and boundary conditions for the above governing equations are

$$t = 0; \quad T = T_0 \quad 0 \le r \le r_s \tag{11}$$

$$T = T_\infty, \quad Y_F = 0, \quad Y_O = Y_{O_\infty} \quad r_s < r \tag{12}$$

$$r = 0; \quad \frac{\partial T}{\partial r} = 0 \tag{13}$$

$$r = \infty; \quad T = T_\infty, \quad Y_F = 0, \quad Y_O = Y_{O_\infty} \tag{14}$$

at the evaporation front; $r = r_{li}(t)$

$$\rho_g D_O \frac{\partial Y_O}{\partial r}\bigg|_+ = \rho_g V Y_O \tag{15}$$

$$-\rho_g D_F \frac{\partial Y_F}{\partial r}\bigg|_+ = \rho_g V(1 - Y_F) \tag{16}$$

$$\frac{dr_{li}}{dt} = -\frac{\dot{m}}{4\pi c \rho_l r^2}\bigg|_{r=r_{li}} - \frac{\int_0^{r_{li}} \varepsilon \frac{\partial \rho_l}{\partial t} r^2 \, dr}{[\varepsilon \rho_l r^2]_{r=r_{li}}} \tag{17}$$

where

$$\dot{m} = \frac{4\pi r^2}{L}\left(q|_+ - \lambda_{sl}\frac{dT}{dr}\bigg|_-\right) \tag{18}$$

$c = 1$ and $c = \varepsilon$ represent heating and shell formation stage and pressure build-up stage, respectively,

$$V = \frac{\rho_{li}}{\rho_g}\frac{dr_{li}}{dt} \tag{19}$$

$$Y_F|_{r=r_{li}} = A \, \exp\left[-\frac{(L_0 \times MW)_F}{R_U}\int_{T(r_{li})}^{T_B}\frac{(T_{cr}-T)^a}{T^2}\right. \tag{20}$$

$$\left. dT\right]_{r=r_{li}}$$

$$T|_+ = T|_- \tag{21}$$

at the droplet surface; $r = r_s(t)$

$$\frac{\partial T}{\partial r}\bigg|_- = \frac{q}{\lambda_{sg}}, \quad p = p_\infty \tag{22}$$

Eq. (22) is used only once when the pressure build-up stage is about to take place, namely, when the evaporation front is about to detach from the droplet surface to migrate inward. Subscripts $+$ or $-$ indicate the outward or inward side at the location of interest, respectively. Eq. (17) is a modified form of the equation originally employed by Klingsporn and Renz [19] for application to the slurry droplet. Eq. (20) represents the modified Clausius–Clapeyron equation in that the latent heat of vaporization for liquid fuel is employed as a function of temperature.

The heat flux to the evaporation front, q in Eq. (18) has a different form dependent on whether the evaporating gas passes through the porous region into the gaseous field or directly into the gaseous field, as follows:

During the heating or shell formation stage:

$$q = \lambda_g \frac{dT}{dr}\bigg|_{r=r_s^+} + e_s \sigma(0.53267 T_h^4 - T_s^4) \tag{23}$$

T_h and T_s denote the heaters' wall temperature and the droplet surface temperature. Coefficients in the radiative heat flux term were estimated by considering the view factor between the heaters and the droplet.

During the pressure build-up stage:

$$q = \lambda_{sg} \frac{dT}{dr}\bigg|_{r=r_{li}^+} \tag{24}$$

4. Results and discussion

4.1. Evaporation suppression

Fig. 4 represents a temporal variation of the droplet size for pure *n*-heptane. Here, it is shown that the numerical calculation yields a better agreement with the experimental data when the thermal expansion is taken into consideration. This implies that the thermal expansion of the liquid droplet needs to be considered in the heating process. Starting from about 1.4 s, the droplet size history can be well described by the d^2-law, which represents a linear variation of the square of the droplet diameter with time.

The results presented in Fig. 5 are associated with an unstabilized Al/*n*-heptane slurry droplet. The symbols indicate a variation of experimentally-observed droplet size squared, while the lines indicate the calculated value of the evaporation front. The symbolic marks for rigid shell formation delineate an instant of the evaporation front from the droplet surface. In other words, before the rigid shell formation begins, the drop surface exactly coincides with the evaporation front. Therefore the theoretical lines after the shell formation point represent the radius squared of the wet surface inside the slurry droplet.
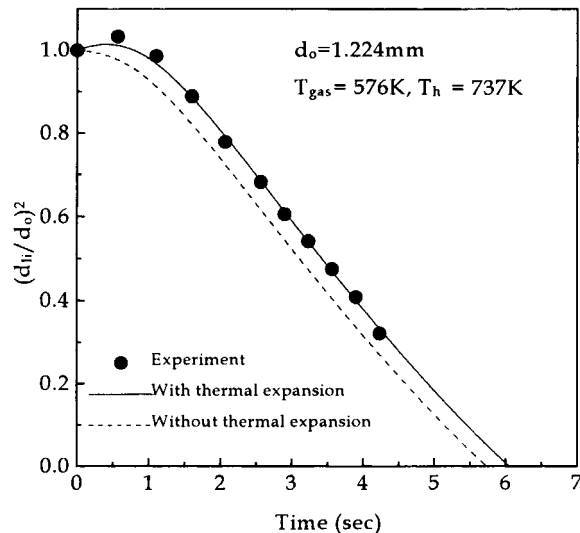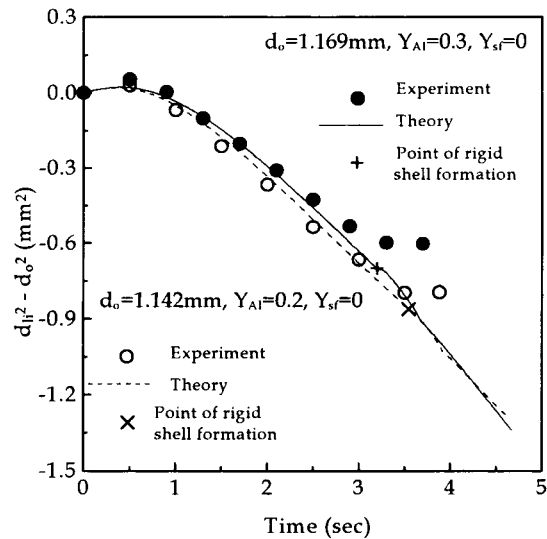
An addition of surfactant and solid particles into

Fig. 5. Temporal change of diameter squared for unstabilized (without surfactant) Al/*n*-heptane slurries with $Y_{sf} = 0$, $Y_{Al} = 0.2$, 0.3, $T_{gas} = 591$ K and $T_h = 778$ K.

liquid fuel droplet usually retards the evaporation rate of liquid fuel alone. Especially when the surfactant molecules establish a thin monolayer near the droplet surface, the diffusive mode of evaporation occurs through this layer. Also, for a slurry droplet, the solid particles accumulated lead to the porous shell formation as evaporation process advances. Due to its limited diffusion through the monolayer and the shell formation, the evaporation rate is reduced as observed by Wong et al. [6]. To account for an extent of evaporation suppression due to the surfactant addition, which is difficult to be modeled theoretically, the suppression factor, A is introduced in the modified Clausius–Clapeyron Eq. (20). While the suppression free condition without surfactant is represented by $A = 1$, $A = 0$ means a complete suppression of liquid carrier due to surfactant. Since the accurate selection of A by using an analytical method is a very formidable problem, a simplified form of A is, here, suggested as follows

$$A = A_i - (A_i - A_f) \times \left(1 - \frac{m_{li}}{m_{li,0}}\right) \tag{25}$$

where A_i and A_f are initial and final suppression factors, respectively. While $m_{li,0}$ is an initial liquid mass, m_{li} is a liquid mass at a time of interest during evaporation. Eq. (25) is devised from a though that the suppression of evaporation would be proportional to the relative amount of surfactant compared with the mass of the liquid carrier during evaporation, while the initial and final suppression factors are empirically deter-

Fig. 4. Experimental and theoretical variation of diameter squared for a pure *n*-heptane droplet.

mined. The initial and final suppression factors, A_i and A_f, are selected as 0.6, and 0.3, from comparison of the experimental and theoretical results.

One additional thing required to be accurately modeled is the prediction of point of rigid shell formation, at which the liquid surface begins to migrate into the interior of the droplet detached from its surface, while the overall droplet size remains constant. In this study, once the accumulated shell thickness reaches its critical value, the rigid shell is considered to be shaped. Here, the critical shell thickness (l_{sh}) is obtained by using Eq. (1) with the experimental droplet size and the porosity,
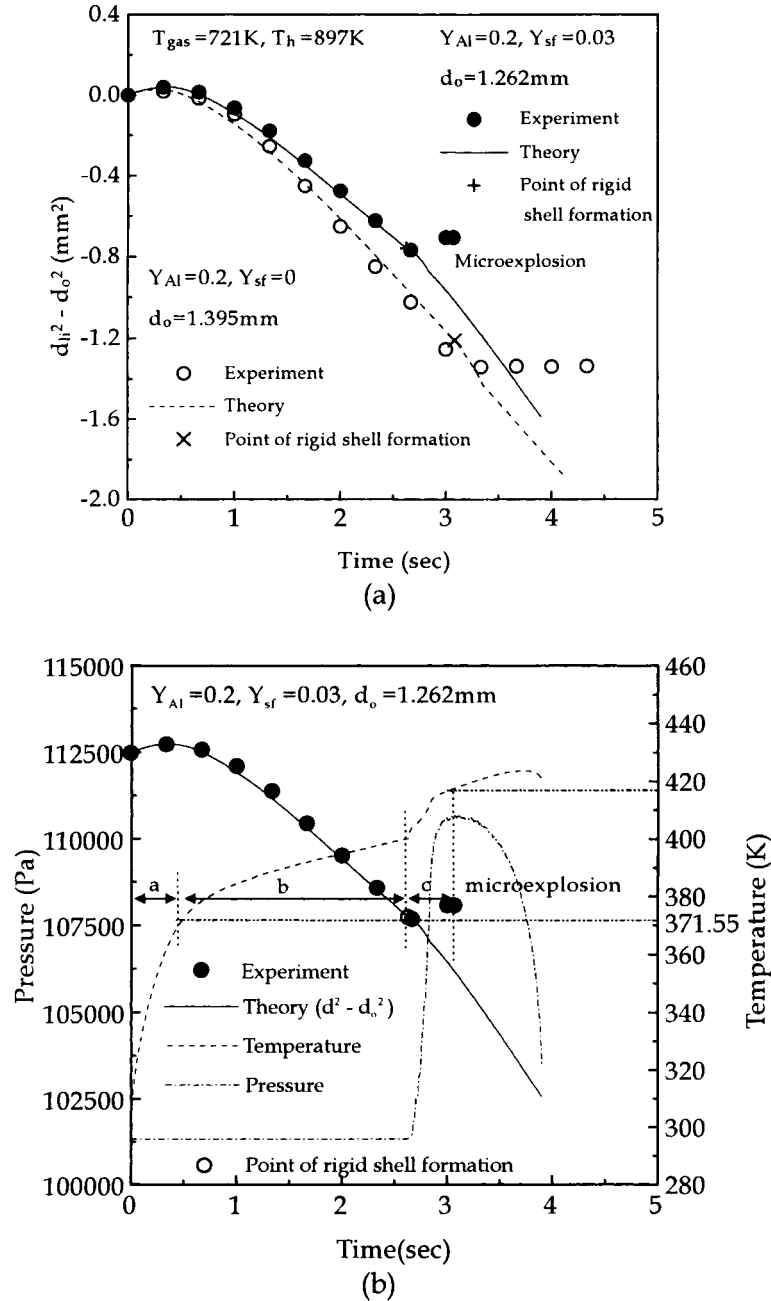

Fig. 6. Experimental and theoretical results for a stabilized Al/n-heptane slurry with $Y_{Al} = 0.2$, $T_{gas} = 721$ K and $T_h = 897$ K. (a) Comparison of d^2 for slurry droplets with/without surfactant. (b) Variations of superheating and pressure build-up at the evaporation front of a stabilized Al/n-heptane slurry (a: heating stage; b: shell formation stage; c: pressure build-up stage).
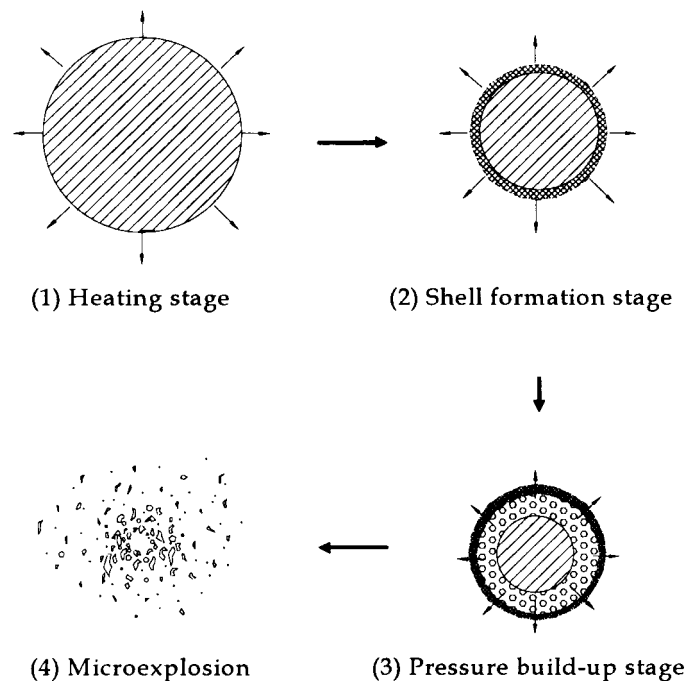
Fig. 7. Microexplosion mechanism of a slurry droplet with surfactant.

$\varepsilon_{sh} = 0.476$ [7]. The porosity of the accumulated shell must lie between the theoretically closest packing condition of 0.260 and the most open packing condition of 0.476 of spheres [7]. A texture in the accumulated shell is supposed to be very close to the most open packing condition, because no external force is being exerted on the shell formation. Therefore, in this work, the most open packing of 0.476 is adopted for the shell porosity [7]. The shell thickness has been assessed by Cho et al. [7], but it is still very difficult to determine it for the case of microexplosion in high temperature, since the shell formation stage is not only obscure, but even the d^2-law period is also ambiguous. In this case l_{sh} is assumed to be about 6 μm which is of the order of one solid particle size following the procedure of Lee and Law [9].

4.2. Shell formation and microexplosion

Based on the experimental observations in this study, the surfactant (SPAN 85) is expected to play a vital role in inducing the microexplosion in slurries. As can be seen in Fig. 6(a), the microexplosion can occur only when surfactant is present (solid circle), otherwise only a rigid agglomerate is formed and sustained during the complete evaporation and combustion duration (open circle). There is also a clear difference in droplet size variation, depending on the existence of

surfactant. The slurry with surfactant is evaporated more slowly than the unstabilized one.

In Fig. 6(b), three stages of microexplosion processes, namely a heating stage, a shell formation stage, and a pressure build-up stage are separately denoted. Its graphical illustration is also depicted in Fig. 7. A heating stage represents the period in which the droplet surface temperature reaches the boiling point of n-heptane. The shell formation stage advances until a rigid agglomerate is formed. During this stage, the variation of droplet diameter squared follows approximately d^2-law. As the droplet shrinks, the solid particles near the droplet surface move along the evaporation front by the surface tension of liquid to form an accumulated shell at the droplet surface. Once the accumulated shell thickness reaches a critical value, the droplet becomes a rigid agglomerate. This is a point of rigid shell formation. Thereafter, the last stage, i.e., a pressure build-up stage begins. Further vaporization of the liquid separates the evaporation front from the rigid droplet surface. Hence, the porous region is formed between the evaporation front and the droplet surface. Because the inter-linking solid particles in the porous region resist the vaporizing gas flow to some extent, a slight increase of pressure can be achieved in this porous region.

The porous shell consisting of particle layers accumulated near the surface resists the flow of liquid fuel vapor so that a pressure increase follows.
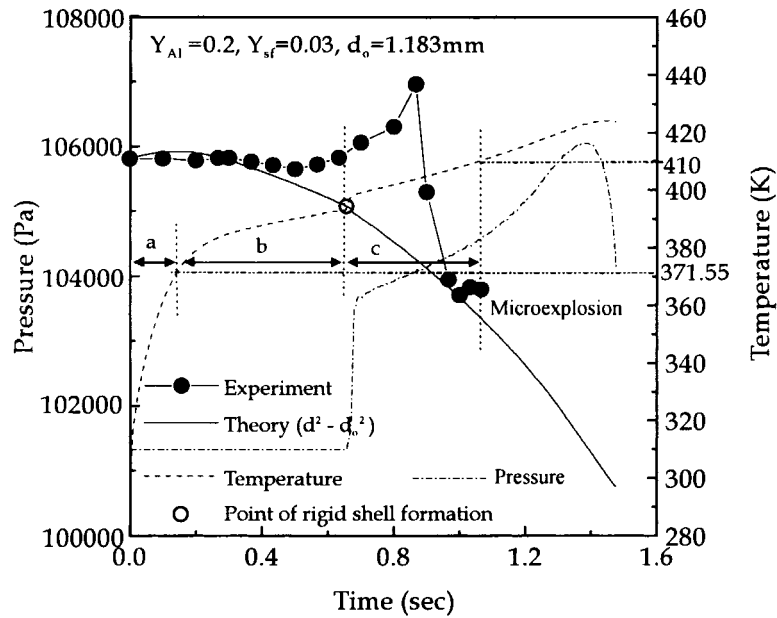
(a)
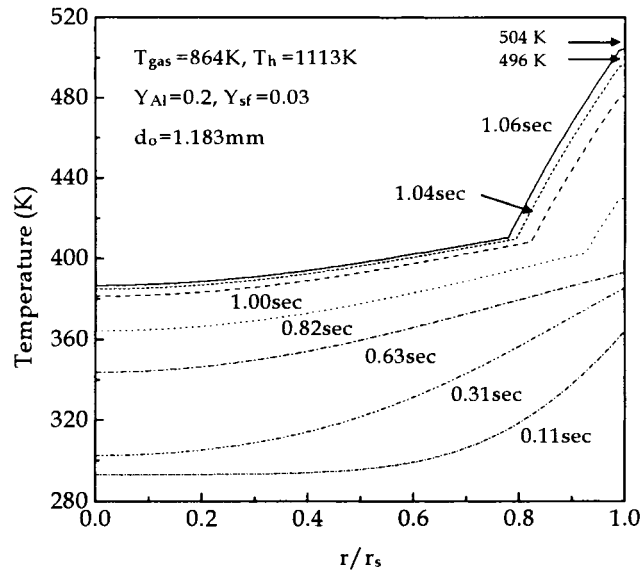
(b)

Fig. 8. Experimental and theoretical results for a stabilized Al/*n*-heptane slurry with $Y_{Al} = 0.2$, $Y_{sf} = 0.03$, $T_{gas} = 864$ K, $T_h = 1113$ K and $d_o = 1.183$ mm. (a) Superheating and pressure build-up at the evaporation front (a: heating stage; b: shell formation stage; c: pressure build-up stage). (b) Internal temperature distributions.

Simultaneously, the shell temperature can exceed the boiling point of the liquid fuel, reaching the surfactant pyrolysis temperature. Consequently, the pressure build-up in the shell is rapidly prompted, since the surfactant pyrolysis renders the shell texture less permeable to the fuel vapor. Therefore, this stage in the present study is called the pressure build-up stage, in comparison with the shell formation stage mentioned by Takahashi et al. [3,4].

A temperature variation of the liquid layer front inside the droplet is also plotted in Fig. 6(b). The superheating stage is achieved by the fact that an additional heating of the droplet becomes possible due to the evaporation suppression by the surfactant. An abrupt change of the temperature gradient in liquid layer front right after the end of rigid shell formation in Fig. 6(b) results from the pressure rise inside the droplet which, then, induces an increase in the liquid boiling temperature. It is noticeable in Fig. 6(b) that the temperature of the liquid surface reaches about 418 K just prior to microexplosion, which is approximately regarded as the heterogeneous nucleation temperature for this slurry droplet with n-heptane. The pressure variation at the evaporation front is also depicted in Fig. 6(b), which indicates the pressure build-up due to the resistance to the vaporized gas flow in the porous region.

Wong and Lin [5] took the criterion for the initiation of disruption as the time when the temperature at the position $r = 0.8r_s$ reaches the boiling point of liquid fuel according to experimental results. Takahashi et al. [3,4] and Cho et al. [7] suggested that the disruption can occur when the droplet surface temperature reaches the surfactant pyrolysis temperature using the TGA results. However, since this surfactant pyrolysis temperature can vary depending on defining the weight fraction pyrolysed, in this study, instead, possibility of using the limit of superheat for heterogeneous nucleation as a criterion for microexplosion is investigated.

Fig. 8(a) shows the experimental as well as theoretical results for the stabilized Al/n-heptane slurry when exposed to a higher heater temperature ($T_h = 1113$ K) compared with the results in Fig. 6. In Fig. 8(a), it is noticeable that the droplet size history does not follow the d^2-law in the shell formation stage and a significant swelling of the droplet is observed due to its fast pressure build-up. The time duration required for the shell formation stage is also relatively reduced compared with the others, giving more time to the pressure build-up stage. This is ascribed to the rapid evaporation, because of this, the surface tension of the liquid cannot easily drag the particles as the evaporation front radially shrinks, since each aluminum particle essentially has a large inertia. This situation becomes more aggravated by the mutual bonding of solid par-
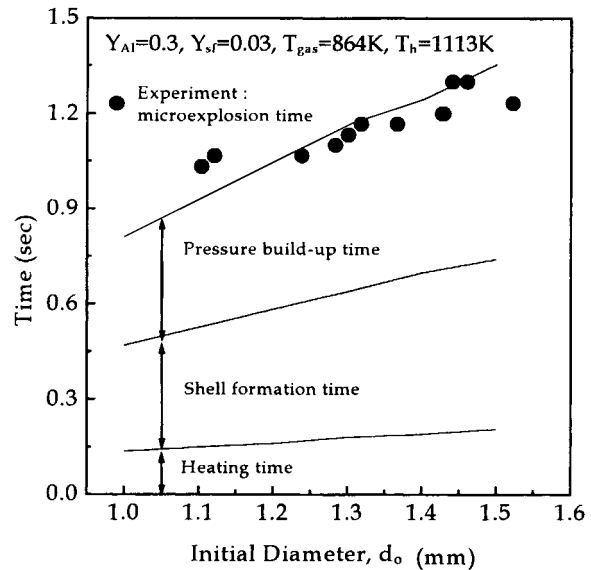

Fig. 9. The effect of initial diameter on microexplosion time for $Y_{Al} = 0.3$, $Y_{sf} = 0.03$, $T_{gas} = 864$ K and $T_h = 1113$ K.

ticles due to surfactant addition. After a relatively thin shell is formed, the slurry droplet can be exploded due to heterogeneous nucleation in the same way as in Fig. 6. In Fig. 8(a), it is noted that the temperature at the evaporation front just prior to microexplosion attains 410 K, which is close to 418 K in Fig. 6(b).

For a multicomponent liquid droplet, the microexplosion mechanism is postulated in terms of homogeneous nucleation inception. That is, the more volatile component, which is trapped in the core of the droplet due to diffusional resistance by a less volatile component, can be heated up to the state at which homogeneous nucleation becomes possible [20]. From the experimental results by Sinitsyn and Skripov [21], the limit of superheat for homogeneous nucleation of n-heptane is found to be about 487 K, which is much higher than its boiling point of 371 K. For heterogeneous nucleation, the surface characteristics such as catalyst, promote nucleation much more easily. Even on a plane surface, the limit of superheat is reduced by approximately 30% if a contact angle is 90° [21]. Therefore, the nucleation temperature is approximately above the boiling point and below the 450 K. The typical temperature is now taken as a criterion by which the microexplosion time can be assessed. In Fig. 8(b), the internal temperature distribution is plotted. In this figure, the shell surface temperature reaches 504 K at the moment of microexplosion and 496 K at the moment of disruption, which is above the surfactant pyrolysis temperature of 492 K. Takahashi et al. [3,4] and Cho et al. [7] suggested that disruption can occur when the droplet surface temperature reaches the sur-

factant pyrolysis temperature and used the temperature as criterion of disruption. The result in Fig. 8(b) also shows the possibility of using the surface temperature as criterion for the disruption. In this study, instead, heterogeneous nucleation temperature is used as a criterion for microexplosion. Even if more work is clearly needed to characterize the heterogeneous nucleation temperature in the porous media, 410 K is taken as the heterogeneous nucleation temperature here as previously mentioned from the comparison between experimental and theoretical results.

4.3. Microexplosion times

The theoretical model is also used to predict a microexplosion time for stabilized slurries. As previously mentioned, it is defined as the time required for the liquid surface of a droplet to reach the heterogeneous nucleation temperature, 410 K. Fig. 9 shows the effect of initial droplet diameter on the microexplosion time for slurry droplets with 30 wt.% of aluminum particles. The simulation yields a reasonable agreement with the experimental data. In general, the larger the initial droplet size, the longer the microexplosion time becomes, for the overall process is retarded for the larger droplet size. It is also seen that the shell formation time is comparable to the pressure build-up time, while the heating time is comparatively smaller than the others. The effect of initial solid loading on the microexplosion time is plotted in Fig. 10. The microexplosion time is seen to decrease as the initial solid loading increases. This results from the fact that as the solid loading increases, the shell formation time significantly decreases, even if the heating and pressure build-up times increases, as shown in the figure. While the shell formation stage, in which a densely-packed particle layer is formed near the droplet surface, is considered to be substantially affected by the solid loading itself, the heating and pressure build-up stages are considered to be affected by the thermal properties of the solid loading. The thermal conductivity of the slurry droplet would increase as the solid loading increases, which results in the more uniform temperature inside the droplet. Thereby, more time is necessary for both heating and pressure build-up stages. It must be noted that the pressure build-up is related to the heating of the liquid up to the superheated state. However, it is also observed that the effect of solid concentration is gradually diminished as the rate of shell formation time decreases and it converges to a certain limiting value. This fact coincides with the observation by Wong and Turns [2].
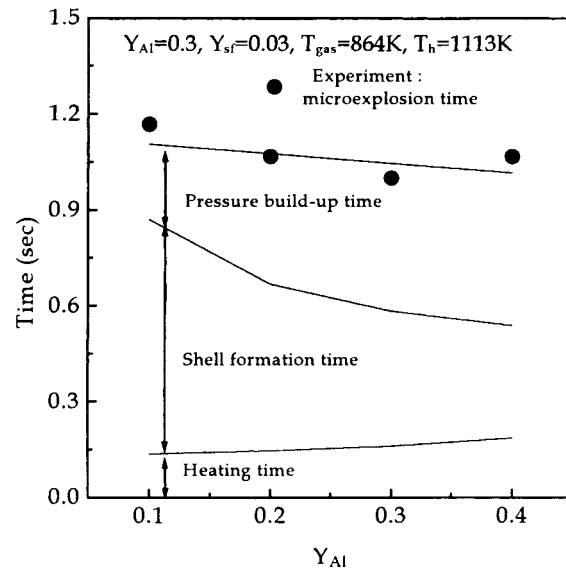

Fig. 10. The effect of initial solid loading on microexplosion time for $Y_{sf} = 0.03$, $T_{gas} = 864$ K, $T_h = 1113$ K and $d_o = 1.2$ mm.

5. Conclusions

A theoretical as well as experimental investigation was completed to study the microexplosion process for slurry droplets with 10 to 40 wt.% of aluminum particle loading at several ambient temperatures. For a stabilized slurry droplet, it was found that the surfactant not only inter-links solid particles near the droplet surface to cause the rigid shell formation, but it also suppresses the evaporation of the liquid carrier, which finally leads to the superheating of the liquid over its boiling point. Thereby, the heterogeneous nucleation resulted in the microexplosion.

In the numerical simulation, the suppression factor as well as the pressure build-up in the porous region of the droplet is taken into consideration. As an onset of microexplosion, the heterogeneous nucleation was defined by considering the limit of superheat of liquid and the existence of solid particles. A reasonably good agreement with the experimental data for droplet variation and microexplosion time could be obtained for various initial droplet sizes and particle loading. In addition, three stages in microexplosion process are identified and quantitatively estimated to figure out their relative importance.

References

[1] S.C. Wong, S.R. Turns, Ignition of aluminum slurry droplets, Combustion Science and Technology 52 (1987) 221–242.

[2] S.C. Wong, S.R. Turns, Disruptive burning of aluminum/carbon slurry droplets, Combustion Science and Technology 66 (1989) 75–92.

[3] F. Takahashi, F.L. Dryer, F.A. Williams, Combustion behavior of free boron slurry droplets, in: Twenty-First Symposium (International) on Combustion, The Combustion Institute, Pittsburgh, 1986, pp. 1983–1991.

[4] F. Takahashi, I.J. Heilweil, F.L. Dryer, Disruptive burning mechanism of free slurry droplets, Combustion Science and Technology 65 (1989) 151–165.

[5] S.C. Wong, A.C. Lin, Microexplosion mechanisms of aluminum/carbon slurry droplets, Combustion and Flame 89 (1992) 64–76.

[6] S.C. Wong, A.C. Lin, H.Y. Chi, Effects of surfactant on the evaporation, shell formation and disruptive behavior of slurry droplets, in: Twenty-Third Symposium (International) on Combustion, The Combustion Institute, Pittsburgh, 1990 pp. 1391–1397.

[7] S.Y. Cho, F. Takahashi, F.L. Dryer, Some theoretical consideration on the combustion and disruption of free slurry droplets, Combustion Science and Technology 67 (1989) 37–57.

[8] S.C. Wong, A.C. Lin, C.E. Wu, Microexplosions of boron and boron/carbon slurry droplets, Combustion and Flame 96 (1994) 304–310.

[9] A. Lee, C.K. Law, Gasification and shell characteristics in slurry droplet burning, Combustion and Flame 85 (1991) 77–93.

[10] T.Y.R. Lee, R.E. Taylor, Thermal diffusivity of dispersed materials, ASME Journal of Heat Transfer 100 (1978) 720–724.

[11] R.A. Ahmad, E.C. Mathias, S. Boraas, Gaseous oxygen cooling of the space transportation system launch pad environment, Journal of Spacecraft and Rocket 28 (6) (1991) 689–697.

[12] T. Elperin, B. Krasovitov, Evaporation of liquid droplets containing small solid particles, International Journal of Heat and Mass Transfer 38 (1995) 2259–2267.

[13] D. Kunii, J.M. Smith, Heat transfer characteristics of porous rocks, AIChE Journal 6 (1960) 71–78.

[14] R.C. Reid, J.M. Pausnitz, B.E. Poling, The Properties of Gases and Liquids, 4th ed., McGraw-Hill, New York, 1987.

[15] F.A. Williams, Combustion Theory, The Benjamin/Cummings Publishing Company, Inc, 1985.

[16] W.M. Rohsenow, J.P. Hartnett, E.N. Ganic, Handbook of Heat Transfer Fundamentals, 2nd ed., McGraw-Hill, New York, 1985.

[17] T. Saitoh, O. Nagano, Transient combustion of a fuel droplet with finite rate of chemical reaction, Combustion Science and Technology 22 (1980) 227–234.

[18] K. Raznjevic, Handbook of Thermodynamic Tables and Charts, Hemisphere, 1976.

[19] M. Klingsporn, U. Renz, Vaporization of a binary unsteady spray at high temperature and high pressure, International Journal of Heat and Mass Transfer 37 (1994) 265–272.

[20] C.H. Wang, X.Q. Liu, C.K. Law, Combustion and microexplosion of freely falling multicomponent droplets, Combustion and Flame 56 (1984) 175–197.

[21] R. Cole, Boiling nucleation, Advances in Heat Transfer 10 (1974) 104.